EasyChair Preprint

№ 13292

Towards HVDC Interoperability - Neutral Current Control for Multiple Terminals

Dong Chen, Pimonpan Phurappa, Benjamin Marshall, Mohammad Wasim Ahmad and Callum Henderson

May 15, 2024

Towards HVDC Interoperability - Neutral Current Control for Multiple Terminals

Dong Chen*[1]
dong.chen@sse.com

Pimonpan Phurappa[1,2]
Peach.Phurappa@sse.com
P.Phurappa@sms.ed.ac.uk

Benjamin Marshall[1]
Benjamin.Marshall@sse.com

Mohammad Wasim Ahmad[1]
MohammadWasim.Ahmad@sse.com

Callum Henderson[1]
callum.henderson@sse.com

***Abstract*— This paper proposes a novel control strategy to eliminate the neutral currents of multiple bipolar terminals in a multi-terminal-multi-vendor HVDC grid. Assisted by DC symmetrical decomposition, the proposed control over neutral current is decoupled from power transfer without the need for access to internal design of converters. A generic mathematical model is derived to quantify the robustness against measurement error of DC current without detailing internal design of converters. Through comparisons between 3 types of Pseudo-steady State simulations with MATLAB/Simulink and Electro-Magnetic Transient (EMT) simulation in the Real Time Digital Simulation (RTDS) environment, the outcomes confirm the applicability of the proposed methodology and feasibility of controlling selected neutral currents for a multi-terminal-multi-vendor HVDC grid.**

Keywords—HVDC, Interoperability, Neutral current control, DC symmetrical decomposition, Robustness

I. INTRODUCTION

Towards the Net-zero target of Great Britain, multi-terminal High Voltage Direct Current (HVDC) grid has been deemed as an enabler of massive utilization of off-shore wind power in the North Sea [1].As a trail-blazer, Project Aquila has been launched to develop the first offshore multi-vendor-multi-terminal HVDC grid [2].

To improve reliability against loss of the transfer branch and reduce the insulation stress against earth, bipolar scheme has been proposed for Aquila project [2][3]. When a Dedicated Metallic Return (DMR) cable is fitted in a bipolar transfer section, up to half of its transfer capability can be preserved in the case of loss of one pole. However, such an arrangement becomes too costly for those long transmission sections, which might not pass a cost-benefit-assessment. As a result, hybrid schemes of both full bipolar arrangement (with DMR) and rigid bipolar (without DMR) are expected to be inter-connected in future HVDC grids to balance cost and reliability [3].

When a bipolar DC grid is fully balanced between poles, the current carried by neutral lines is zero as the currents of positive and negative poles will ideally cancel each other in every section [4]. However, when one pole is lost in a full bipolar section, the network impedance between two poles is no longer symmetrical. Such imbalance will give rise to propagation of unbalanced components throughout the network and thus non-zero neutral currents will be induced accordingly.

Due to environmental regulations in GB, the earthing path is not permitted to carry current during steady state. Thus, active control is expected to eliminate the neutral current of a rigid bipolar section even with significant network imbalance [3], typically when one terminal loses a pole end within the network. To make the problem more challenging, vendors will not provide access to the internal controls of the HVDC converter despite that control interactions, which all neutral currents are related to, are inevitable. Therefore, it is expected that a neutral current control solution can be designed by transmission system operators with specifiable performance of HVDC converters without infringing the intellectual property of vendors in the internal design of the converters. So far, it is also unclear if such neutral current control can be achieved without compromising the performance of control over power transfer.

Further concerns are extended to the robustness when neutral current controls are applied to multiple rigid bipolar sections. As the neutral currents of rigid bipolar sections are expected to be zero, the steady state errors of neutral current are thus expected to be zero. Concerns were drawn with a symmetrical comparison with the well-known design of DC voltage droops for interconnecting multiple DC terminals when regulating their local voltages with steady state errors [5]. Eliminating steady state error for radially-connected terminals may lead to excessive current deviation carried by transfer branches in response to measurement error of DC voltage. It is unclear if multiple neutral current controls with such requirement will lead to significant voltage variations or even voltage collapse when they are coupled by one DC network.

To address the industrial challenges above, this paper proposes a simple solution to neutral current control for multi-vendor-multi-terminal HVDC. It features as follows:

1. With the assist of DC symmetrical decomposition, a neutral current control strategy is proposed and can be decoupled from power transfer when various types of terminal control are simultaneously implemented.
2. The neutral current control can be decentralized (or centralized) and is allowed to be simultaneously implemented by multiple DC terminals.
3. The control is embedded into secondary feedback control, whose outputs feed into standardized control interfaces of "black-boxed" converters to allow interoperability.
4. An analytical model is derived for the proposed control and related combinations of control strategy to quantify the sensitivity against measurement error at 0 Hz.

The rest of the paper is organized as followed. The proposed control and its analytical model are introduced in Section II. It is followed by robustness assessment in Section III. After that, case studies are presented in Section IV with the conclusion drawn in Section V.

1. *The National HVDC Centre, Scottish Hydro Electric Transmission,* Cumbernauld, UK
2. *Industrial Centre for Doctoral Training in Offshore Renewable Energy (IDCORE), University of Edinburgh, Edinburgh, UK*

II. Modelling and Control Strtegy

A. Representation of Bipolar HVDC System with Symetrical Decomposition

Within a multi-terminal bipolar HVDC grid, each terminal can be represented by a bipolar shunt branch, which is as Fig. 1(a) shows. The instantaneous values of terminal voltage and current of a bipolar terminal can be represented by the space vectors:

$$\vec{V_\iota} = [v_{i+}, v_{i-}]^T \tag{1}$$

$$\vec{I_\iota} = [i_{i+}, i_{i-}]^T \tag{2}$$

, which are the space vectors of voltage and current of *i*-th terminal, respectively. The letter " i" used in the subscript indicates the labelling number of the terminal, whereas the notion of "+" and "-" represent the positive and negative polarity of the variable.

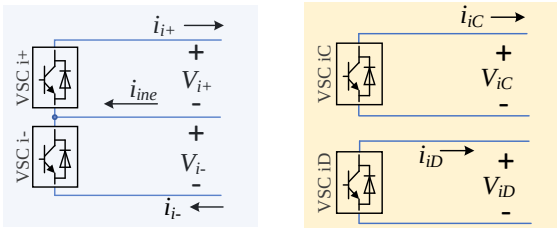

(a) "+-" frame (b) CD frame

Fig. 1. Representation of Bipolar Terminal *i*

Thus, v_{i+}, v_{i-} are the voltages of the positive and negative poles of *i*-th terminal, respectively; for a radial network, i_{i+}, i_{i-} are defined as the currents carried by the positive and negative poles as well as the branches of *i*-th terminal, respectively. And the neutral current carried by the neutral line is defined as:

$$i_{ine} = i_{i+} - i_{i-} \tag{3}$$

To regulate the neutral current of a selected terminal and then decouple this function from power transfer, DC symmetrical decomposition [3][6][7] is proposed to be adopted to decouple the components related to neutral current control from power transfer, where a constant power transformation is adopted and the transformation matrix is [3]:

$$T = \frac{1}{\sqrt{2}}\begin{bmatrix} 1 & 1 \\ 1 & -1 \end{bmatrix} \tag{4}$$

With this constant power transformation, the matrix is orthogonal such that the following stands

$$T = T^T = T^{-1} \tag{5}$$

In this new reference frame, termed as "CD" frame in this paper, where the subscript of "CD" refers to the space vector of "C" being common-mode and "D" being (differential-mode). the voltage and currents can be represented by:

$$\begin{cases} \overrightarrow{V_{\iota CD}} = T\vec{V_\iota} = [v_{iC}, v_{iD}]^T \\ \overrightarrow{I_{\iota CD}} = T\vec{\iota_\iota} = [i_{iC}, i_{iD}]^T \end{cases} \tag{6}$$

The equivalent circuit of *i*-th terminal in CD frame is shown in Fig. 1(b). Considering (3)(4)(6), the neutral current can be represented in the CD reference frame as

$$i_{ine} = \sqrt{2} i_{iD} \tag{7}$$

Remark 1: in some literature, similar components of C and D are regarded as "residual phase sequence" and "balanced phase sequence", respectively, using non-orthogonal transformation matrix [7]. For convenience of derivations brought by (5), transformation matrix in (4) is adopted in this paper.

When the system is linearized at 0 Hz, the conductance matrix $G_{iT} = T\vec{V_\iota} = [v_{iC}, v_{iC}]^T$ of the *i*-th terminals is defined as

$$G_{iT}\vec{V_\iota} = \vec{I_\iota} \tag{8}$$

Substituting (5)(6) into (8), one can write

$$G_{iTCD}\overrightarrow{V_{\iota CD}} = \overrightarrow{I_{\iota CD}} \tag{9}$$

, where G_{iTCD} is the terminal conductance in CD frame as

$$G_{iTCD} = TG_{iT}T \tag{10}$$

More broadly, for a bipolar HVDC network of *n* terminals, whose network conductance matrix G_{net} complies nodal analysis as

$$\begin{cases} G_{net}\vec{V} = -\vec{I_t} \\ G_{netCD}\overrightarrow{V_{CD}} = -\overrightarrow{I_{tCD}} \end{cases} \tag{11}$$

, where

$$\begin{cases} \vec{V} = [\vec{V_1}^T, \vec{V_2}^T, \cdots, \vec{V_n}^T]^T \\ \vec{I_t} = [\vec{I_1}^T, \vec{I_2}^T, \cdots, \vec{I_n}^T]^T \end{cases} \tag{12}$$

$$G_{netCD} = T_n G_{net} T_n \tag{13}$$

$$\begin{cases} \overrightarrow{V_{CD}} = T_n\vec{V} \\ \overrightarrow{I_{tCD}} = T_n\vec{I_t} \end{cases} \tag{14}$$

and T_n is a $2n \times 2n$ transformation matrix as

$$T_n = diag\{T, T, \cdots, T\} \tag{15}$$

B. Control Architecture and Representation of Terminals

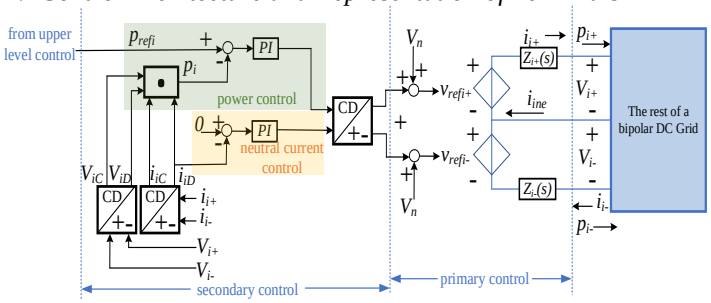

Fig. 2. Terminal Control Architecture

Without requiring the internal design of each converter, each shunt branch with primary control is proposed to behave as a controllable voltage source behind a synthesis impedance in the s-domain as Fig. 2 shows, where the order of voltage source serves as the control interface for the secondary control to update [8].

In this paper, the secondary control includes power control and neutral current control, which collectively update the input orders of the controllable voltage source of every primary control in Fig. 2.

C. Terminal Conductance Matrix

To quantify the measurement robustness against zero-drifting, a complete analytical model of bipolar HVDC grids must be obtained at 0 Hz. As an essential step, the conductance matrix of the terminal under various combinations of control modes is derived in this section.

1) Terminal with primary control only

As shown in Fig. 2, when the secondary control is not updating the control interface to the primary control of the *i*-th terminal, the dynamics of the terminal exposed to the rest of the grid is determined by the primary control, i.e., the voltage droop control. Referring to Fig. 2, the corresponding conductance matrix in "+-" reference frame is

$$G_{iT} = \begin{bmatrix} 1/Z_{i+}(s) & 0 \\ 0 & 1/Z_{i-}(s) \end{bmatrix}|_{s=0} = \begin{bmatrix} k_{i+} & 0 \\ 0 & k_{i-} \end{bmatrix} \quad (16)$$

, where $Z(s)$ is the synthesis impedance of one pole end in s-domain and k is its reciprocal response at 0 Hz.

2) Terminal with power control and neutral current control

As shown in Fig. 2, when the D component of current is eliminated by the integral regulator with a feedback control and the system is assumed stable, the 0 Hz response of the terminal is equivalent to the one with its neutral line open-circuited. Referring to Fig. 1(b), the D-component of conductance is 0 and the terminal conductance matrix in CD frame is

$$G_{iTCD} = \begin{bmatrix} \frac{\partial I_{iC}}{\partial V_{iC}} & 0 \\ 0 & 0 \end{bmatrix}|_{s=0} = \begin{bmatrix} \frac{\partial (p_{iC}/V_{iC})}{\partial V_{iC}} & 0 \\ 0 & 0 \end{bmatrix} = \begin{bmatrix} \frac{-p_{iC}}{V_{iC}^2} & 0 \\ 0 & 0 \end{bmatrix} \quad (17)$$

, where p_{ic} is the total power delivered by the C-component circuit in Fig. 1(b) such that

$$p_i = p_{iC} + V_{iD}I_{iD} = V_{i+}I_{i+} + V_{i-}I_{i-} = V_{iC}I_{iC} + V_{iD}I_{iD} \quad (18)$$

Assuming $I_{iD} = 0$ when neutral current control is effectively eliminating the neutral current at steady state, (18) can be approximated as

$$p_{iC} \approx V_{i+}i_{i+} + V_{i-}i_{i-} \quad (19)$$

Substituting (4)(5)(6)(17)(19) into (10), one can solve the corresponding matrix of terminal conductance in "+-" frame as

$$G_{iT} = \frac{-V_{i+}i_{i+} - V_{i-}i_{i-}}{(V_{i+}+V_{i-})^2}\begin{bmatrix} 1 & 1 \\ 1 & 1 \end{bmatrix} \quad (20)$$

3) Terminal with neutral current and primary control

When the primary control is cascaded by neutral current control as the outer loop, the conductance elements in the D-component are forced to be 0 to form the corresponding conductance matrix in CD frame such that

$$G_{iTCD} = T\begin{bmatrix} k_{i+} & 0 \\ 0 & k_{i-} \end{bmatrix} T^* \begin{bmatrix} 1 & 1 \\ 0 & 0 \end{bmatrix} = \frac{1}{2}\begin{bmatrix} k_1 + k_2 & k_1 - k_2 \\ 0 & 0 \end{bmatrix} \quad (21)$$

, where "*" denotes the operator of bit wise product (Hadamard product). Thus, the corresponding conductance matrix in "+-" frame can be obtained by substituting (4)(21) into (10) as

$$G_{iT} = \frac{1}{2}\begin{bmatrix} k_1 & k_2 \\ k_1 & k_2 \end{bmatrix} \quad (22)$$

III. Quantifying Robustness at 0 Hz

To assess the propagation and amplification of measurement error against the neutral current control, a complete grid conductance matrix, which counts both the terminal conductance and network conductance, is needed.

A. Grid conductance of a bipolar HVDC grid

The conductance matrix of an *n*-terminal grid, *G*, is a $2n \times 2n$ matrix, and can be obtained by substituting (8)(12) into (11) as [8]

$$F = (G_{net} + G_T)\vec{V} = G\vec{V} = 0 \quad (23)$$

, where *F* is defined as a function of equilibrium constraint, G_T is the $2n \times 2n$ conductance matrices of all shunt branches of bipolar terminals, i.e., the converters:

$$G_T = diag\{G_{1T}, G_{2T}, \cdots, G_{nT}\} \quad (24)$$

, and $G_{net} = \{G_{net,ij}\}$ is the $2n \times 2n$ conductance matrix of the transfer network, whose elements are [3]

$$\begin{cases} G_{net,ij} = -M_{i,j} & (i \neq j) \\ G_{net,ii} = \sum_{j=1,i\neq j}^{n} M_{i,j} \end{cases} \quad (25)$$

, where $M_{i,j}$ is the 2×2 conductance matrix block of the bipolar transfer branch between *i*-th and *j*-th terminal (j = 1, 2, ⋯, n) as

$$M_{i,j} = \frac{1}{R_{ij+}R_{ij-}+R_{ij+}R_{ijN}+R_{ij-}R_{ijN}}\begin{bmatrix} R_{ij-} + R_{ijN} & R_{ijN} \\ R_{ijN} & R_{ij+} + R_{ijN} \end{bmatrix} \quad (26)$$

, where R_{ij+}, R_{ij-} and R_{ijN} are the resistances of the positive, negative, and neutral line of the transfer branch, respectively.

B. Robustness against Measurement of Neutral Current

The voltage variation induced by measurement errors of neutral current control can be quantified by the small-signal sensitivity function between the neutral current and terminal voltage.

Perturbating the dynamics between terminal voltage and nodal current with the equilibrium function *F* in (23), the small-signal conductance at 0 Hz can be represented by the Jacobian matrix of the *F* function with respect to the voltage vector $\vec{V}$ as

$$G\Delta\vec{V} = \Delta\vec{I} \quad (27)$$

, where $\Delta\vec{V}$ is the *2n*-dimension vector of perturbation voltage at all pole ends and $\Delta\vec{I}$ is the *2n*-dimension vector of response current injected into all pole nodes. When the $2n \times 2n$ resistance matrix *R* is defined as

$$R = G^{-1} \quad (28)$$

Therefore, it can be inferred from (27)(28) that

$$R\Delta\vec{I} = \Delta\vec{V} \quad (29)$$

Applying the "+-/CD" transformation in (6) to the current vector in (29), one can write the sensitivity function between current in CD reference frame and voltage in "+-" reference frame as

$$R(T_nT_n)\Delta\vec{I} = RT_n\Delta\overrightarrow{I_{CD}} = \Delta\vec{V} \quad (30)$$

, where the elements of the even rows in RT_n (corresponding to all D components) reflects the sensitivity. Considering (7), and substituting (23)(28) into (30), the actual sensitivity function against measurement error of the neutral current at *i*-th terminal can be characterized by the elements of 2*i*-th rows of R^* ($i = 1, 2, \cdots n$) as

$$R^* = \frac{-1}{\sqrt{2}}(G_{net} + G_T)^{-1}T_n \quad (31)$$

, whose 2*i*-th row and *j*-th column ($j = 1, 2, \cdots, 2n$) elements reflects the amplification of the voltage at *j*-th terminal node against the measurement error of neutral current at *i*-th terminal.

Remark 3: (29) can capture 0-Hz dynamics of hybrid controls in both CD frame and "+-" frame. Further robustness against error of voltage detection and disturbances between various mapping between vectors of inputs and outputs can be derived similarity. Similar methodologies can also be extended with other control designs, but they are left for future reporting.

Remark 4: since the proposed neutral current control is designed to virtually open the circuit of the shunt branch of the applied bipolar terminal, at least one bipolar terminal should not adopt neutral current control. This is to ensure no measurement error of neutral current be applied to an infinite value of aggregated resistance, which will lead to system collapse.

IV. Case Studies

To verify the performance of the proposed control and the sensitivity to measurement error, a benchmark system is set up as shown in Fig. 3 with initial parameters in TABLE I.

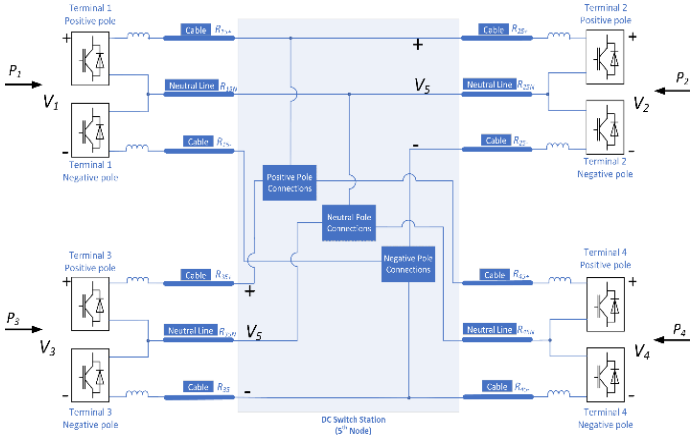

Fig. 3. Layout of 4-Terminal-5-Node Benchmark System

All 4 terminals are interconnected via a DC switch station as the 5th Node with positive, negative, and neutral lines the transfer branches.

All transfer branches between each bipolar terminal and the junction point, i.e., a switching station, are identical. To introduce a significant imbalance, an extra resistance of 200 Ω is inserted between positive poles of Terminals 1 and 5 (the junction switching station).

Two types of Pseudo-steady State (PS) models, analytical mode at 0 Hz and an Electro-Magnetic Transients (EMT) model are compared with time-domain simulations. Pseudo-steady state models and analytical model are simulated with MATLAB/Simulink, whereas the Real-Time Digital Simulator (RTDS) is used for the EMT simulation. All control and circuits are bound to converge to steady state, i.e., s = 0 in the transfer functions for the pseudo-steady model, which will be further introduced in the following sections; whereas in EMT models, generic average HB-MMC models are used with inter-arm and inter-phase balancing control included [9]. Besides, similar frequency dependent models of DC cables [10] are used to simulate DC links in EMT simulations.

A. Model Configurations and Simulated Case

1) Configurations for the Pseudo-steady State (PS) simulation

Pseudo-steady State simulations are implemented by 3 types of modelling appraoches to characterized the system depicted in Fig. 3:

Approach a) With full closed-loop structure of secondary control

All transfer branches, including neutral lines, are modelled as resistors. Referring to Fig. 2, all dynamics of primary control are modelled as resistors. Secondary controls, i.e., neutral current control and power control, are implemented as feedback loops. This modelling approach is to verify if the control structure of the neutral current control can lead to an equilibrium with selected neutral currents settling at zero without compromising control over power transfer.

TABLE I. Initial Parameter of the Benchmark System

Parameter	Symbol	Value
Power Electronics and Cable Impedances		
Impedance of the Positive Pole Cable from Terminbal 1 to the Switch Station	$R_{15\pm}$	205.5 Ω
Polarity Line Impedances	$R_{25\pm}$, $R_{35\pm}$, $R_{45\pm}$	5.5 Ω
Neutral Line Impedances	R_{15N}, R_{25N}, R_{35N}, R_{45N}	5.5 Ω
MMC Conduction Resistance for EMT Simulation (per arm)	Z_G	0.56 Ω
Valve Capacitance (per arm)	C	43.5 μF
Control Parameters		
Rated Voltage (bipolar)	V_{Rated}	1050 kV
Droop Gains (equivalent to bipolar)	$K_{1\pm}$, $K_{2\pm}$, $K_{3\pm}$, $K_{4\pm}$	8.258 A/kV
Timesteps of PS Simulation (Tustin/ Backward Euler)	Δt_{PS}	100 μs
Timesteps of EMT Simulation (Dommel)	Δt_{EMT}	50 μs
HB-MMC Parameters		
Current Loops Bandwidth per pole of with respect to an infinite AC bus connection	B_{CL}	600 Hz
Control frequency	f_{CL}	20 kHz
Time Constant for DC Voltage Lead Regulators	T_{Lead}	0.004 s
Time Constant for DC Voltage Lag Regulators	T_{Lag}	0.02 s

Approach b) Neutral current control modelled as neutral line open:

Modifying a), the model of the neutral current control is replaced by opening the neutral line of every corresponding terminal. This is to represent ideal performance of the neutral current control for comparison with Approach a) and analytical approach.

Approach c) Analytical Approach:

Starting from an existing equilibrium. the incremental voltages at all pole ends in response to a step change of a measurement error are computed using (31). This model is to predict the impact of small-signal input at 0 Hz. In this paper, interest is placed on error of current measurement.

2) Configurations for the EMT Simulation.

Corresponding to Fig. 3, all MMCs are half-bridge and represented by an identical EMT average model, whereas the cables of transfer branches are represented by a frequency dependent model. Lead-lag regulators are cascaded with every voltage droop regulator in primary control. All converters and its

transfer branches connecting to the DC switch station in Fig. 3 are identical, except for the fore cited extra resistor injected to the positive pole branch of Terminal 1. The EMT model is simulated by RTDS in real time.

In this case study, all combinations of control modes in section II.C are included in the benchmark system. Terminal 1 and 4 are the terminals with primary control only, i.e., secondary control disabled. Terminal 2 is assigned as a constant power terminal with proportional gain of power regulator at 0.1 kV/MW and time constant at 0.001 s along with the neutral current control with proportional gain of 314 Ω with the same time constant in the secondary control, corresponding to the complete control architecture in Fig. 2. Terminal 3 consists of the neutral current control cascading the primary control only.

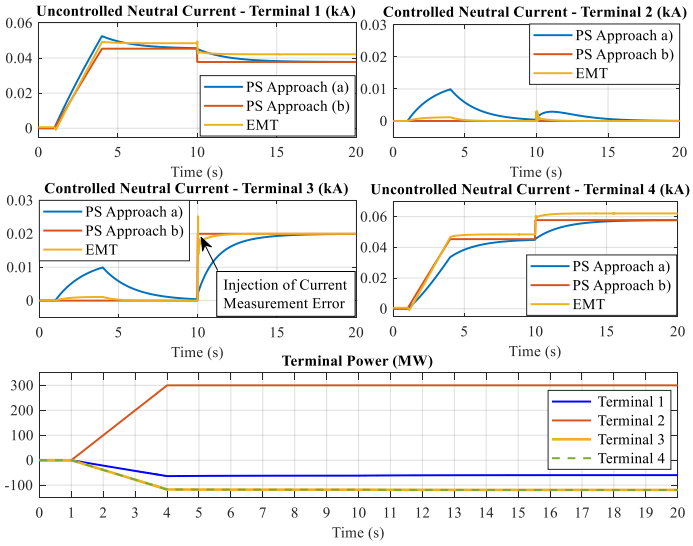

Fig. 4. Neutral Currents and Terminal Powers of each Terminal

3) Stages of the Case

a) Initiation: No-load condition at time (t) = 0 – 1 s

b) Power ramp: A power ramp of 100 MW/s is applied to Terminal 2 from t = 1 s until P_{ref2} = 300 MW. This is to shift equilibrium to test modelling accuracy against operating power, which introduces non-linearity in impedance.

c) Constant power rebalancing: As shown in Fig. 4, the remaining three terminals begin rebalancing the power system at the same timestep (t = 1 s). Due to a loss of the positive pole, Terminal 1 contributes approximately 63 MW at a steady state which is only half as much to the power accommodation process. Meanwhile, Terminal 3 and 4 facilitate the rebalancing at the same scale (118.5 MW at a steady state) as the droop coefficients and network metrics are symmetrical.

d) Noise current injection: After P_{ref2} is accommodated and the system reaches a steady state, a step change of error, is applied to the neutral current measurement at Terminal 3 at t = 10 s.

B. *Comparisons between the Pseudo-steady State Simulation and the EMT Simulation*

Illustrated in Fig. 5, the investigation picks up the profiles of voltage to verify the sensitivity performance and prediction against measurement error. The negative pole of Terminal 3 is specifically chosen due to the measurement error injected at the negative pole of Terminal 3, while Terminal 1 is selected as a representative of a distant terminal away from the occurrence of measurement error in a neutral line at Terminal 3.

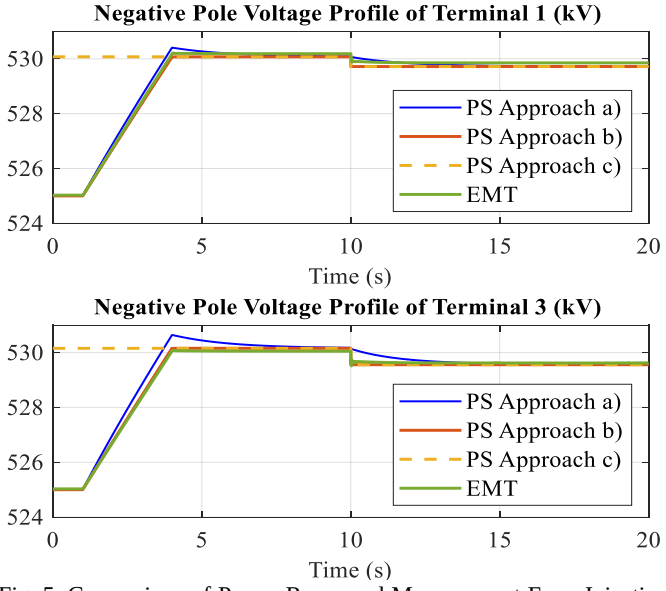

Fig. 5. Comparison of Power Ramp and Measurement Error Injection between PS and EMT Simulations

At the initiation state, all terminals are operating at 0 MW. The voltage at both terminals remains at the nominal value of 525 kV. With the decrease in power at Terminal 1 during the rebalancing process, the negative voltage at Terminal 1, V_{1-}, escalates from its nominal value. Once the first steady state is reached at t = 10 s, V_{1-} approximately converges at 530.1 kV. This value is utilised as the operating voltage for the analytical model, represented by the dashed lines in Fig. 5. The negative voltage at Terminal 3, V_{3-}, follows the same trend and settles at 530 kV upon the first steady state.

At t = 10 s, the measurement error of 20 A is injected to the neutral line of Terminal 3. To maintain the constant power, both V_{1-} and V_{3-} decrease to approximately 529 kV at a new steady state. The response voltages at Terminal 1 of the full bipolar configuration in the PS and EMT simulations are 0.355 kV and 0.335 kV, respectively. Meanwhile, the negative pole voltages at Terminal 3 decline by 0.598 kV and 0.427 kV for the PS and EMT models with the same full bipolar arrangement, respectively. The precise values of each terminal voltages to 3 decimal places are included in TABLE II.

The completion of the power ramp and power rebalancing between t = 1 s to t = 10 s and the settling neutral currents of Terminal 2 and 3 at 0 kA (see Fig. 4) show that the proposed neutral current control can effectively eliminate the steady state error, while being decoupled from the function of the power dispatch.

TABLE II. TERMINAL VOLTAGES AT STEADY STATES BEFORE AND AFTER THE MEASUREMENT ERROR INJECTION OF THE NEUTRAL CURRENT

Negative Pole Voltages in	**Terminal 1**	**Terminal 3**
The First Steady State at Stage *c)*		
PS Approach a) – feedback loops modelled for secondary control	530.142 kV	530.256 kV

Negative Pole Voltages in	Terminal 1	Terminal 3
PS Approach b) – neutral line open for neutral current control representation	530.073 kV	530.157 kV
PS Approach c) – analytical	530.073 kV	530.157 kV
EMT – RTDS	530.187 kV	530.051 kV
The Second Steady State after Error Injection - Stage *d)*		
PS Approach a) – feedback loops modelled for secondary control	529.720 kV	529.563 kV
PS Approach b) – neutral line open for neutral current control representation	529.717 kV	529.559 kV
PS Approach c) – analytical	529.718 kV	529.559 kV
EMT – RTDS	529.852 kV	529.624 kV

As per Table II, the comparison between the EMT simulation and the Pseudo-steady State simulations reveals a close alignment in operating point, with errors consistently lower than 0.03% for Terminal 1 and below 0.13% for Terminal 3 throughout the simulations.

The comparison also shows that results of all pseudo-steady approaches aligned with each other in the settling point. More specifically, the alignment of settling points between Pseudo-steady State Approach a) with Approach b) shows that the proposed control over neutral current is equivalent to opening the neutral branch when the system settles to steady state. The overlapping between Pseudo-steady State Approach b) and Approach c) shows that the derived analytical model in Section II and III does capture the system dynamics with multiple neutral current controls at 0 Hz.

The incremental voltages in response at local (Terminal 3) and remote terminals (Terminal 1) to the 1% current measurement error are less than 1% of the rated voltage (525 kV), which shows that this error is hardly amplified or propagating despite of two terminals (Terminal 2 and 3) are both employing integral regulators to control neutral currents. This indicates the feasibility of good robustness against the zero drifting of measurement errors when implementing multiple neutral current controls.

Despite of the good alignment in operating point across various modelling approaches, the prediction of incremental response to the measurement error shows a level of deviation between pseudo-steady state and EMT, i.e., approximately 5% at remote end and 29% at local end. Given the losses of converter, which can alter the equivalent resistance/conductance of DC terminal in (16)(20)(21), are not captured in pseudo-steady state approaches whilst a good margin offered by the low per-unit amplification ratio in both local and remote ends, it is envisaged that it will not compromise the sufficiency of robustness against measurement error.

V. Conclusions

This paper represents further control methodologies built upon a UK patent (2307888.4.) established in Ref [3]. The proposed neutral current control can effectively eliminate neutral current of selected bipolar terminals in a radial HVDC network despite of significant imbalance of network resistance.

Decoupling "CD" components for rigid bipolar terminals and natural "+-" components for full bipolar simultaneously in secondary control, the proposed neutral current control can be decoupled from DC power transfer.

The stability basis of the proposed neutral current control at 0 Hz may be mathematically derived and monitored within a controller, whilst protecting the intellectual property of vendors. The approach of various control modes integration at the secondary level, cascading the voltage droop control in the primary level, is therefore quantifiable against neutral current measurement error at 0 Hz. Results from four time-domain simulation approaches, in pseudo-steady state and EMT, show it is possible to contain the amplification or propagation of such errors.

The effectiveness of the control also implies an enhanced operational flexibility attainable in a multi-terminal HVDC system such that the increase of grid capacity after loss of one pole end can be positively correlated with the increase of bipolar terminals in future projects, which is subject to future report.

Acknowledgment

The paper is funded by Project Aquila via UK Net Zero Acceleration allowance and partially supported by Industrial Centre for Doctoral Training in Offshore Renewable Energy (IDCORE) via the grant EP/S023933/1 from the UK Engineering and Physical Sciences Research Council (EPSRC) and the UK Natural Environment Research Council (NERC).

References

[1] HM Government Department for Business, Energy & Industrial Strategy, "Net Zero Strategy: Build Back Greener", Policy paper, Oct. 2021. Accessed: May 13, 2024. [Online]. Available: https://www.gov.uk/government/publications/net-zero-strategy

[2] The National HVDC Centre, "Aquila Interoperability Package – The National HVDC Centre". Accessed: May 13, 2024. [Online]. Available: https://www.hvdccentre.com/our-projects/aquila-interoperability-package/

[3] D. Chen and B. Marshall, "Modelling Asymmetrical HVDC Transfer Network for Multi-Vendor-Multi-Terminal Interoperability", *IET Powering Net Zero Week 2023 - Renewable Power Generation*, Glasgow, UK, Nov. 2023.

[4] S. De Boeck et al., "Configurations and earthing of HVDC grids," *2013 IEEE Power & Energy Society General Meeting*, Vancouver, BC, Canada, 2013, pp. 1-5.

[5] B. K. Johnson, R. H. Lasseter, F. L. Alvarado and R. Adapa, "Expandable multiterminal DC systems based on voltage droop," *IEEE Trans. on Pow. Del.*, vol. 8, no. 4, pp. 1926-1932, Oct. 1993

[6] Y. Gu, W. Li and X. He, "Analysis and Control of Bipolar LVDC Grid With DC Symmetrical Component Method," in IEEE Transactions on Power Systems, vol. 31, no. 1, pp. 685-694, Jan. 2016.

[7] Thomas Westerweller, "HVDC Grid Text Book," Siemens Energy Global, 1st Edition, Grid Technologies, Siemenspromenade 1191058 Erlangen, Germany, pp. 17-20 Unpublished

[8] D. Chen *et al.*, "Towards HVDC interoperability - assessing existence of equilibrium with reference to converter terminal behaviour," *19th International Conference on AC and DC Power Transmission (ACDC 2023)*, Glasgow, UK, 2023, pp. 224-231.

[9] D. Guo *et al.*, 'Detailed quantitative comparison of half-bridge modular multilevel converter modelling methods', *J. Eng.*, vol. 2019, no. 16, pp. 1292–1298, 2019.

[10] J. Beerten, S. D'Arco, and J. A. Suul, 'Frequency-dependent cable modelling for small-signal stability analysis of VSC-HVDC systems', *IET Gener. Transm. Distrib.*, vol. 10, no. 6, pp. 1370–1381, 2016.